International Journal of Heat and Mass Transfer 55 (2012) 6846–6853

Contents lists available at SciVerse ScienceDirect

International Journal of Heat and Mass Transfer

journal homepage: www.elsevier.com/locate/ijhmt

Steady-state heat conduction analysis of solids with small open-ended tubular holes by BFM

Xianyun Qin [a], Jianming Zhang [a,*], Luping Liu [b], Guangyao Li [a]

[a] State Key Laboratory of Advanced Design and Manufacturing for Vehicle Body, College of Mechanical and Vehicle Engineering, Hunan University, Changsha 410082, China
[b] Hydrochina Zhongnan Engineering Corporation, Changsha 410014, China

ARTICLE INFO

Article history:
Received 1 March 2012
Received in revised form 24 June 2012
Accepted 29 June 2012
Available online 24 July 2012

Keywords:
Heat conduction
Tubular hole
Boundary integral equations
Boundary face method
CAD model

ABSTRACT

In this work, the boundary face method (BFM) is applied to implement steady-state heat conduction analysis of solids containing a large number of open-ended tubular shaped holes of small diameters. A new meshing scheme is used to discretize the boundary integral equations (BIE) such that the holes can be modeled by a small number of surface elements while keeps the exact geometry, resulting in substantial savings in both modeling effort and computational cost. In the scheme, each tubular pipe surface is represented with a number of curvilinear tube elements similar to the 'hole element' proposed by P.K. Banerjee. To model the end faces that are intersected by the tubular holes, a special triangular element with negative parts is proposed. These elements are defined in the parametric space of the surface, and the exact geometry data can be directly available from CAD models of the solids. Numerical examples show that current implementation is very efficient in modeling of solids with many holes of arbitrary shape. The temperature and flux on the pipe surfaces or inside solids are obtained with high accuracy, even the local thermal concentration on and near the holes can be captured.

1. Introduction

Structures containing many slender tubular shaped holes find important application in engineering, such as cooling passages, electrical wiring passages, etc. For instance, in concrete construction process, many water pipes are embedded to cool down the dam. These pipes have significant influences on the resulting temperature and flux distribution in a body and thus draw much attention of the design engineers to properly arrange these pipes.

The temperature and flux distribution in bodies with holes is complicated and can only be understood with numerical methods, such as the finite element method (FEM) or the boundary element method (BEM). In numerical analysis of the problems related to these bodies, two main difficulties arise. The first one is modeling of small holes with arbitrary shape. The second is accurately capturing the local thermal concentration caused by the holes. A FEM discretization of the domain would be extremely complicated to perform, especially when the diameters of the tubular holes are very small, which may be of a lower scale than domain size. In addition, the FEM requires a very fine mesh to accurately capturing the local thermal concentration, which may beyond the current computing power.

Alternatively, the BEM has some distinct advantages over the FEM for analyzing the problems involving the complicated geometries, such as a surface discretization instead of the domain discretization and thermal gradients can be captured more accurately. However, in a conventional BEM analysis, modeling a small hole still requires a very fine surface mesh. The fine mesh leads to a large-scale computational cost. For a free shaped tubular hole, it is a challenging task to generate surface elements with a suitable quality. To simplify mesh generation as well as get a better efficiency, a lot of efforts have been made [1–7]. The common idea behind those works is developing different kinds of approximation formulations of the BEM. The excellent work has been taken by Banerjee et al. [2–7], in which the special formulation has been developed by using the proposed 'hole element'. Using the hole element, the two-dimensional integration over the surface of the hole is reduced to a one-dimensional line integration along its length by carrying out an analytical integration in the circumferential direction. The pipe with circular cross section can be modelled by a small number of hole elements, resulting in substantial saving in both data preparation and computing cost. Unfortunately, this formulation is under an assumption that the concerned hole is axisymmetric in shape, thus suitable for straight cylindrical or conical holes [3,4]. For curved pipes with variable diameters along their longitudinal direction, there will be a problem in using the formulation.

In this paper the boundary face method (BFM) [8,9] is introduced to analyze steady-state heat conduction problems of solids

* Corresponding author. Tel.: +86 731 88823061.
E-mail address: zhangjianm@gmail.com (J. Zhang).

0017-9310/$ - see front matter © 2012 Elsevier Ltd. All rights reserved.
http://dx.doi.org/10.1016/j.ijheatmasstransfer.2012.06.091

containing tubular shaped holes. In our implementation, all holes are represented with parametric forms, which can be directly derived from original CAD models of the solids. The two-dimensional integrals over the surface of the hole are directly computed in a numerical manner. A new type of surface element is developed in numerical integration, in which the same trigonometric functions from 'hole elements' is used. As a consequence, neither fine traditional surface elements nor 'hole elements' are required for modeling small holes. The holes with complex geometries, such as the high variation of the curvature long its length and the arbitrary shaped cross section, can be described at an easy rate in the BFM. In addition, the 'hole elements' cannot consider the case where the holes intersect with the outer surface of the body, and thus, in the previous works [1–6], the holes of practical structures are treated as blind holes approximately. This treatment will introduce local errors. In this paper, a new type of discontinuous boundary elements with negative parts is designed to describe the ends of the through holes.

This paper is organized as follows. The boundary integral equation formulation with end-opened tubular holes is firstly introduced. This is followed by developing special surface elements for modeling of these holes. Next, numerical examples for sample problems are presented. Finally, the paper ends with conclusions in Section 5.

2. Boundary integral equation formulation with end-opened tubular holes

The BFM is a new implementation of the boundary node method (BNM) or BEM [9–14]. The boundary integral equations (BIE) are commonly used in both methods. However, the BFM is implemented based on CAD model with the boundary representation (B-rep) data structure, in which all bounding surfaces are represented in parametric forms. Both boundary integration and variable approximation are performed in the parametric space of the concerned surface. The details of the implementation for the BFM can be found in Refs. [8,9].

The self-regular BIE for steady-state heat conduction problems is applicable in an analysis of a body containing end-opened tubular holes. This equation can be expressed as

$$0 = I^O + I^H + I^V \tag{1}$$

where

$$I^O = \int_{\Gamma^O} [G(\mathbf{s},\mathbf{y})(T(\mathbf{s}) - T(\mathbf{y})) - F(\mathbf{s},\mathbf{y})q(\mathbf{s})]d\Gamma^O(\mathbf{s}) \tag{2}$$

$$I^H = \sum_{m=1}^{M} \int_{\Gamma_m^H} [G(\mathbf{s},\mathbf{y})(T(\mathbf{s}) - T(\mathbf{y})) - F(\mathbf{s},\mathbf{y})q(\mathbf{s})]d\Gamma_m^H(\mathbf{s}) \tag{3}$$

$$I^V = \sum_{k=1}^{K} \int_{\Gamma_k^V} [G(\mathbf{s},\mathbf{y})(T(\mathbf{s}) - T(\mathbf{y})) - F(\mathbf{s},\mathbf{y})q(\mathbf{s})]d\Gamma_k^V(\mathbf{s}) \tag{4}$$

in which:

T and q are boundary temperatures and fluxes;
$\mathbf{y}$ is the source point and $\mathbf{s}$ is the field point on the boundary;
G and F are the fundamental solutions of the 3D potential problems [8];
Γ_m^H is the surface of the mth hole;
Γ_k^V is the kth triangular element with negative parts created by open-ended holes;
Γ^O is the out surface of the body exception for the elements with negative parts;
I^O denotes the integrals over the Γ^O;
I^H and I^V denote the integrals over the summation of the Γ_m^H and Γ_k^V, respectively;
M and K are the total number of the holes and the elements with negative parts, respectively.

In the conventional discretization of Eq. (1), a very fine surface mesh is required for the efficient modeling and analysis of holes. In our implementation, the hole is represented by a small number of slender surface elements which are defined in the parametric space of the surface of the hole. The geometric information of the hole is directly derived from its parametric surface of its CAD model [9]. This is a distinguishing advantage over the BEM, in which the surface elements are defined in physical space, and the hole is approximated by those elements. In addition, the parametric surface elements are generated without much effort. If a surface is not trimmed, the surface can be meshed easily using isoperimetric lines. As most of tubular holes are represented with no trimmed surfaces, there is no difficulty of meshing those surfaces.

The holes concerned in this paper are open-ended (through holes), and intersect the outer surfaces of the body. The treatment for this type of hole is troublesome and uneconomical in the BEM, and so far no literatures are found about dealing with those holes. Actually, in BEM analysis these holes are simplified as blind holes usually and each hole is closed at the end by a circular disc [1–6]. In this paper, a family of triangular boundary elements with negative parts is proposed. Negative parts are designed specially to represent the ends of the through holes. Using these special elements, the end faces intersected by holes can also be meshed by a small number of surface elements.

After discretization of Eq. (1) using surface elements, the numerical integration of all integrals is carried out by the same program codes, which are developed with the integration techniques in Refs. [8,9]. It is not required to pay additional attention to integrals over small holes, such as an offset from the pipe surface to the pipe central line is made for each node located at the pipe surface [3]. This special treatment will introduce local errors.

3. Special surface elements for modeling of end-opened tubular holes

3.1. Tube element

As mentioned previously, the hole can be represented by a number of slender surface elements with parametric from. This type element is referred to as 'tube element' here, which is an extension of the 'hole element' proposed by Banerjee and Henry et al. [3–6]. A hole, even without circular or elliptical section, can be represented by several tube elements exactly in geometry. Fig. 1 shows a slender hole is modelled by four tube elements. This type element shown in Fig. 2(a) is constructed by four isoparametric lines in the parametric space of the hole surface, which is noted by $(\widehat{x},\widehat{y})$ (see Fig. 2(b)). In the space, $\widehat{y}$ is along tube's length, while $\widehat{x}$ is along the circumferential direction taking a value from 0 to 2π.

To perform numerical integration, the following linear transformation is applied to map a tube element into a local coordinate system (ξ,η)

$$\begin{cases} \xi = (\widehat{x} - \widehat{x}_0)/a \quad \xi \\ \eta = (\widehat{y} - \widehat{y}_0/b \end{cases} \quad \eta \in [-1,1] \tag{5}$$

where $\begin{cases} \widehat{x}_0 = (\widehat{x}_2 + \widehat{x}_1)/2 \\ \widehat{y}_0 = (\widehat{y}_2 + \widehat{y}_1)/2 \end{cases}$ and $\begin{cases} a = (\widehat{x}_2 - \widehat{x}_1)/2 \\ b = (\widehat{y}_2 - \widehat{y}_1)/2 \end{cases}$

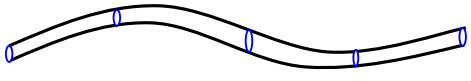

Fig. 1. A tubular hole modelled by four tube elements.

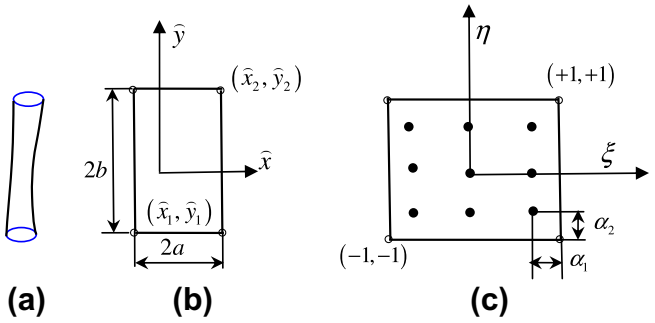

Fig. 2. A tube element, '○' denotes an element vertex and '•' denotes an interpolating node. (a) Element in physical space; (b) element in parametric space of the surface; (c) element mapped into a local coordinate system.

The interpolating nodes are not shared in neighbor elements, thus the variation of approximated field variable is discontinuous between the elements. For each element, the nodes are symmetrically distributed inside it, as shown in Fig. 2(c). An offset from the associated element vertex is taken to locate each node, and the node location is determined by two offset parameters, α_1 and α_2. In this paper, α_1 is taken a value of $\frac{1}{3}$ and $\frac{1}{4}$ for the three nodes and four nodes used in the in circumferential direction, respectively. α_2 is set as $\frac{1}{4}$.

To use the same shape functions from Refs. [4,5,7] in this discontinuous element, two different linear transformations are applied in circumferential and longitudinal directions, respectively. In the circumferential direction, the following transformation from ξ to $\widehat{x}$ is employed

$$\widehat{x} = (\xi + 1.0)\pi - \widehat{x}_0 \tag{6}$$

where $\widehat{x}_0 = \frac{\pi}{3}$ for three nodes used in the direction, and $\widehat{x}_0 = \frac{\pi}{4}$ for four nodes.

Using this transformation, for three nodes, the circular shape functions proposed in Refs. [4,5] are rewritten as

$$\begin{aligned} M^0(\widehat{x}) &= \frac{1}{3} + \frac{2}{3}\cos\widehat{x} \\ M^1(\widehat{x}) &= \frac{1}{3} + \frac{\sqrt{3}}{3}\sin\widehat{x} - \frac{1}{3}\cos\widehat{x} \\ M^2(\widehat{x}) &= \frac{1}{3} - \frac{\sqrt{3}}{3}\sin\widehat{x} - \frac{1}{3}\cos\widehat{x} \end{aligned} \tag{7}$$

The circular shape functions with four nodes, which were first developed by Ref. [7], are expressed as

$$\begin{aligned} M_0(\widehat{x}) &= \frac{(1+\cos\widehat{x}_0}{2}\cos\widehat{x} \\ M_1(\widehat{x}) &= \frac{1}{2} + \frac{1}{2}\sin\widehat{x} - \frac{1}{2}\cos^2\widehat{x} \\ M_2(\widehat{x}) &= \frac{(-1+\cos\widehat{x})}{2}\cos\widehat{x} \\ M_3(\widehat{x}) &= \frac{1}{2} - \frac{1}{2}\sin\widehat{x} - \frac{1}{2}\cos^2\widehat{x} \end{aligned} \tag{8}$$

The linear transformation in the longitudinal direction is expressed as

$$\beta = \frac{\eta}{1.0 - \alpha_2}, \quad \alpha_2 \in (0,1) \tag{9}$$

If a quadratic variation is taken, the shape functions are represented as

$$\begin{aligned} N^0 &= -\tfrac{1}{2}\beta(1-\beta) \\ N^1 &= \tfrac{1}{2}\beta(1+\beta) \\ N^2 &= (1+\beta)(1-\beta) \end{aligned} \tag{10}$$

After dividing the mth hole into N_M number of tube elements together with using the shape functions mentioned above, Eq. (3) can be discretized as

$$\begin{aligned} I_m^H = &\sum_{i=1}^{N_M} \int_{\Gamma_{mi}^H} G(\mathbf{s},\mathbf{y})[M^\alpha(\mathbf{s})N^\gamma(\mathbf{s}) - M^\alpha(\mathbf{y})N^\gamma(\mathbf{y})]T^{\alpha\gamma} d\Gamma_{mi}^H(\mathbf{s}) \\ &- \sum_{i=1}^{N_M} \int_{\Gamma_{mi}^H} F(\mathbf{s},\mathbf{y})M^\alpha(\mathbf{s})N^\gamma(\mathbf{s})q^{\alpha\gamma} d\Gamma_{mi}^H(\mathbf{s}) \end{aligned} \tag{11}$$

in which the subscripts mi is used to denote the ith tube element on the mth hole, $T^{\alpha\gamma}$ and $q^{\alpha\gamma}$ are nodal values of temperature and flux on the surface of the tube element. Summation over α and γ is implied. α ranges from 1 to the number of the nodes in circumferential direction, and γ ranges from 1 to the number of the nodes along the length of the hole.

It should be noticed that in Eq. (11) no geometric approximation is applied. For obtaining geometry exactly, we first obtain the surface parametric coordinates $\widehat{x}$ and $\widehat{y}$ from local integration points using Eq. (5), and then the geometry data is directly calculated from the parametric surface with the parameters: $\widehat{x}$ and $\widehat{y}$. This calculation is completed using the parametric formulation of the surface, which is available from its B-rep data of the CAD model. The temperatures and fluxes on a hole vary in the longitudinal as well as in the circumferential direction, which is exactly the

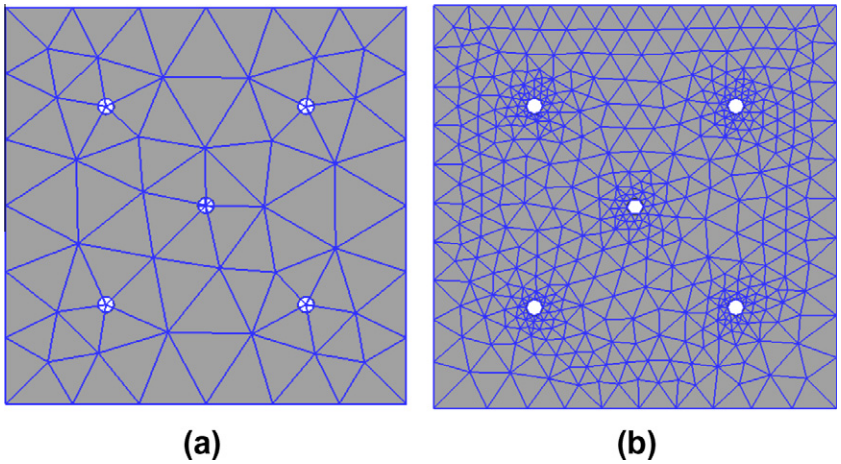

Fig. 3. The two types of meshes for the surface with five small holes. (a) Triangular elements with negative parts. (b) Traditional triangular elements.

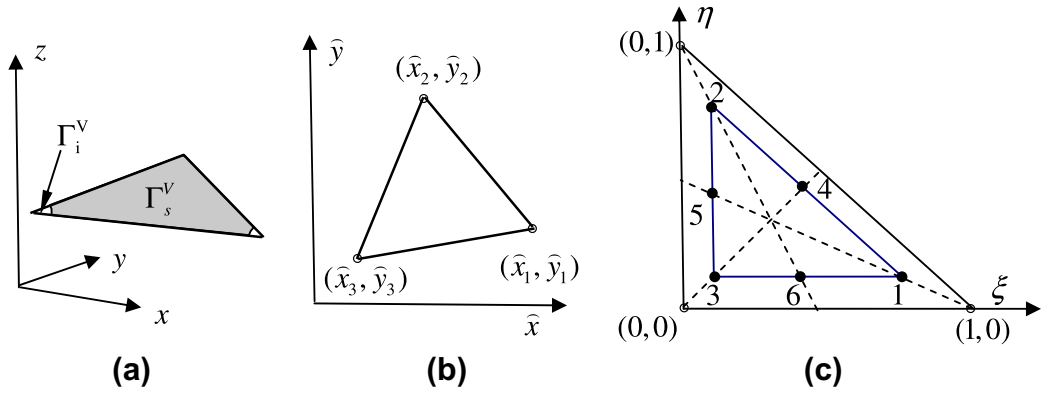

Fig. 4. A triangular element with negative parts. (a) Element in physical space. (b) Element in parametric space of the surface. (c) Element mapped into a local coordinate system.

same as in Refs. [4,5]. For example, the temperature variations can be expressed as

$$T = M^{\alpha}(\mathbf{s})N^{\gamma}(\mathbf{s})T^{\alpha\gamma} \tag{12}$$

3.2. Triangular elements with negative parts

When an open-ended tubular hole intersects an outer surface of the body, the surface is trimmed with small holes. To avoid using a fine mesh to describe each hole, a class of new triangular discontinuous elements with negative parts is developed in this section. The local regions around the hole ends can be meshed with a small number of these elements instead of a large number of traditional elements used in Ref. [9], as illustrated in Fig. 3. Every hole is decomposed as several negative parts, which are located at the corners of the elements around the hole. The center of the hole is coincident with the one of vertices of those elements. Before mesh generation, all centers of the holes are treated as hard points, which are the locations of the nodes in the final mesh. The task of meshing the surface with hard points can be completed in an easy manner with existing meshing techniques. This is why the negative parts are designed at the corners of the elements, not inside them.

Fig. 4 shows a triangular element with two negative parts in different spaces. The negative parts are not drawn in Fig. 4(b) and (c). As the tube element, this element is also defined in the surface parametric space $(\widehat{x},\widehat{y})$ by three or six vertices with parametric coordinates as shown in Fig. 4(b). And Fig. 4(c) depicts the element in the local coordinate system (ξ,η) mapped from the space $(\widehat{x},\widehat{y})$. If three vertices are employed, the following linear map is used from the space (ξ,η) to $(\widehat{x},\widehat{y})$

$$\begin{cases} \widehat{x} = \sum_{i=1}^{3}\phi_i(\xi,\eta)\widehat{x}_i \\ \widehat{y} = \sum_{i=1}^{3}\phi_i(\xi,\eta)\widehat{x}_i \end{cases} \quad \begin{matrix} \xi \\ \eta \in [0,1] \end{matrix} \tag{13}$$

in which $\phi_1 = \xi$, $\phi_2 = \eta$ and $\phi_3 = 1 - \xi - \eta$. Naturally, when six vertices are involved, the quadratic functions of ϕ_i can be available from the traditional boundary elements [1,2], where i from 1 to 6.

When linear interpolation of field variables is taken, three interpolating nodes are used. These nodes are shown in Fig. 4(c) with indices of 1, 2, and 3, which are located at midlines of the triangular element. The local coordinates of the nodes are set by $(0.5\lambda, 0.5\lambda)$, $(1-0.5\lambda, 0.5\lambda)$ and $(0.5\lambda, 1-0.5\lambda)$, respectively. λ is taken a value from 0.1 to 0.4 based on our experience. In this paper, λ are specified as 0.3, and no nodes are located in the negative parts. The triangular patch constructed with the inner nodes is similar to the triangular element. Thus, the new linear interpolating shape functions associated with three nodes can be expressed as

$$\varphi^1 = \tfrac{1}{1-1.5\lambda}(\xi - 0.5\lambda)\ \ \varphi^2 = \tfrac{1}{1-1.5\lambda}(\eta - 0.5\lambda)\ \ \varphi^3 = \tfrac{1}{1-1.5\lambda}(1-\xi-\eta-0.5\lambda) \tag{14}$$

Similarly, the quadratic shape functions with six nodes can be easily obtained as

$$\begin{aligned} \varphi^1 &= a(2a-1) \\ \varphi^2 &= b(2b-1) \\ \varphi^3 &= (1-a-b)(2(1-a-b)-1) \\ \varphi^4 &= 4ab \\ \varphi^5 &= 4b(1-a-b) \\ \varphi^6 &= 4a(1-a-b) \end{aligned} \tag{15}$$

in which $a = \frac{1}{1-1.5\lambda}(\xi - 0.5\lambda)$ and $b = \frac{1}{1-1.5\lambda}(\eta - 0.5\lambda)$. The locations and indices of the six nodes are also shown in Fig. 4(c).

Using the shape functions mentioned above, Eq. (4) for the kth element with N_K number of negative parts can be expressed as

$$\begin{aligned} I_k^V = &\int_{\Gamma_s^V}[G(\mathbf{s},\mathbf{y})(\varphi^{\gamma}(\mathbf{s}) - \varphi^{\gamma}(\mathbf{y}))T^{\gamma} - F(\mathbf{s},\mathbf{y})\varphi^{\gamma}(\mathbf{s})q^{\gamma}]d\Gamma_s^V(\mathbf{s}) \\ &- \sum_{i=1}^{N_K}\int_{\Gamma_i^V}[G(\mathbf{s},\mathbf{y})(\varphi^{\gamma}(\mathbf{s}) - \varphi^{\gamma}(\mathbf{y}))T^{\gamma} - F(\mathbf{s},\mathbf{y})\varphi^{\gamma}(\mathbf{s})q^{\gamma}]d\Gamma_i^V(\mathbf{s}) \end{aligned} \tag{16}$$

where the subscripts s and i refer to the region of the whole element and the region of the ith negative parts of the element, respectively (see Fig. 4(a)), T^{γ} and q^{γ} are nodal values of temperature and flux on the element. Summation over γ is implied, where $\gamma = 1$ to the number of the nodes in the kth element.

In Eq. (16), the initial integrals over the whole element are computed firstly. Then, we obtain the final integrals over the surface region on the element by subtracting the integrals in all negative parts from the initial integrals. In the computing process, the same shapes functions from Eqs. (14), (15) are used. The radius of a negative part is equal to the hole radius, resulting in the size of the negative area is evaluated from the hole data.

4. Numerical applications

The present method has been implemented in a code written in C++ and tested with steady-state heat conduction problems on two different structures: a block with a cylindrical hole and a block with free shaped holes. The first simple structure is used to demonstrate the method capacity of capturing the thermal concentration as well as dealing with holes of very small or larger radii. The second structure, which is more geometrically complicated, is consid-

Table 1
Mesh information, CPU time and memory requirements for the first example.

Model type	Element number	Node number	CPU time (s)	Memory (MB)
BFM with new elements	296	896	2	19.27
Conventional BFM	1490	4470	22	479.58
BEM	1490	4470	21	479.58

ered here to show the advantage of our method in modeling of structures containing a large number of open-ended tubular holes. The conductivity of the two structures is assumed to be 1. All computation are carried out on the same desktop computer with Intel (R) Core(TM)2 Duo CPU (2.33GHz).

4.1. Block with a small cylindrical hole

The first example considers problems in a $10 \times 10 \times 4$ block with an open-ended cylindrical hole. The slender hole is orthogonal to the bottom face $z = 0$ of the block. The central line of the hole passes through the block's center with coordinates (5,5,2). Two cases of the problems are handled regarding to different boundary conditions and a specified radius of the hole.

In the first case, the radius is taken as 0.175. A uniform temperature of 100 °C is applied to the face $y = 0$ of the block parallel to the hole. The opposite face is maintained at a flux of 10. All other faces of the block are insulated. For the purpose of comparison this problem is solved by the present method, the BEM and the conventional BFM without new proposed elements, respectively. The total number of elements and nodes used in the three models are listed in the first and second columns in Table 1. Figs. 5 and 6 show the boundary meshes used in the new BFM and BEM, respectively. The conventional BFM model has the same mesh distribution as in the BEM.

In each computation, the numerical results of fluxes at the internal locations are evaluated. These locations are distributed on the line segment from (0.223,5,2) to (9.770,5,2). The numerical results at the locations are shown in Fig. 7. It is clearly observed that the thermal concentration is explored by the three schemes. The variation of the fluxes obtained by the BFM with proposed elements is in good agreement with that of the conventional BFM and the BEM. It is also found that the same level of the accuracy is obtained by the present method, in which fewer elements (nodes) are used when compared with two other schemes. The comparative results have indicated that the current method can accurately capture the local thermal concentration by a small number of nodes.

The computational requirements of the CPU time and memory used in different models are summarized in Table 1. As expected, the proposed elements allows for a much efficient analysis with substantial savings in both CPU time and memory. The advantage of the proposed elements is likely to be magnified in the problems involved a larger number of holes.

In the second case, the radius of the hole is specified as very small values of 0.025 and 0.0175, compared with the side length of the block. For the block with different radius, Dirichlet problems are solved in which the essential boundary conditions are imposed on all faces corresponding to a cubic reference solution. This solution is expressed as

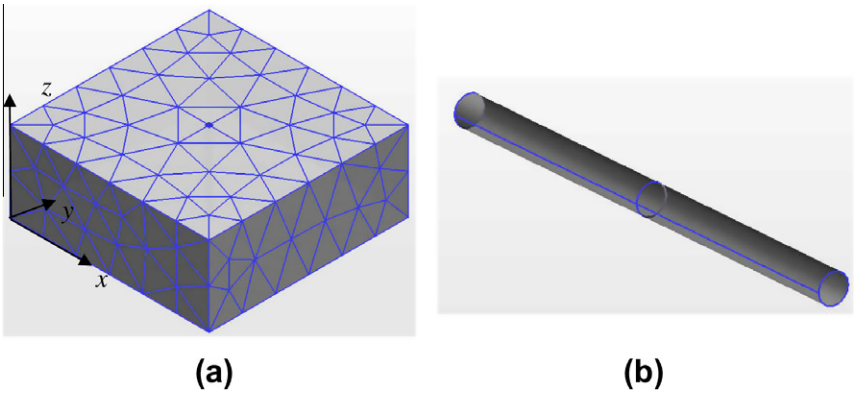

Fig. 5. BFM mesh with proposed elements for a block with a cylindrical hole. (a) Boundary mesh with 296 elements and 896 nodes. (b) The hole modelled with only two tube elements.

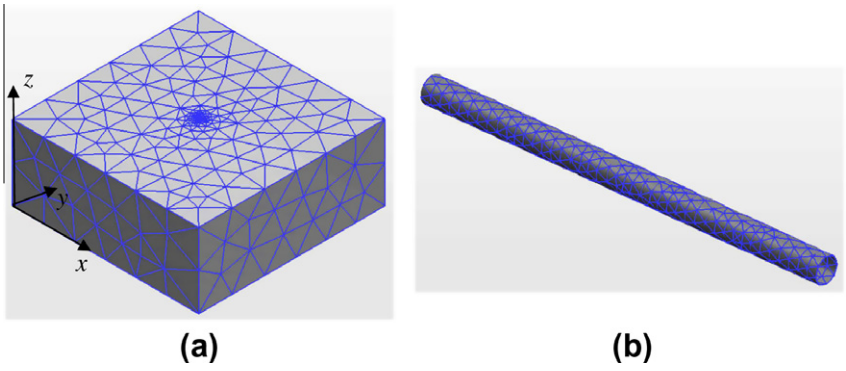

Fig. 6. BEM mesh with traditional elements for a block with a cylindrical hole. (a) Boundary mesh with 1490 elements and 4470 nodes. (b) The hole modelled with fine traditional elements.

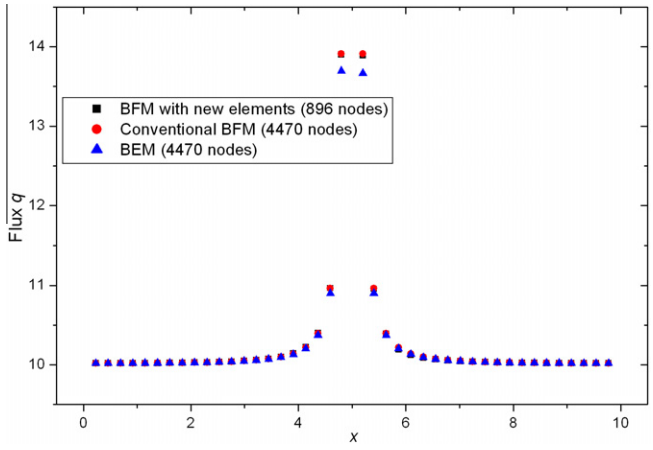

Fig. 7. Variation in flux q along a specified line inside the block with a cylindrical hole.

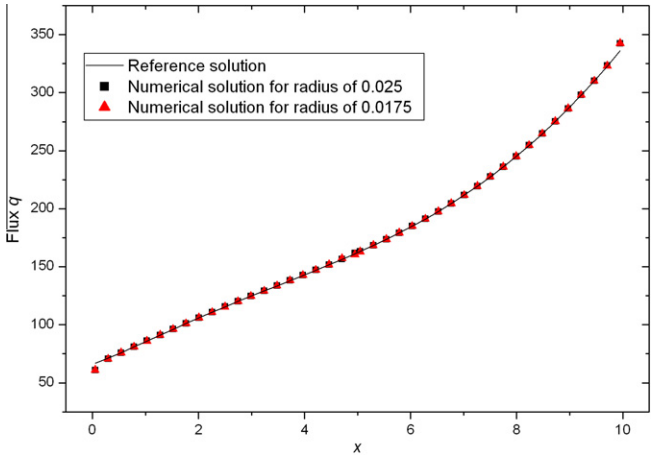

Fig. 8. Variation in flux q along a specified line inside the block with a very small cylindrical hole.

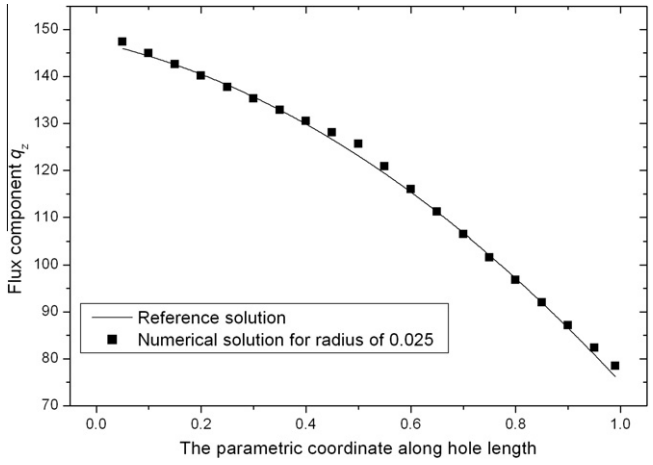

Fig. 9. Variation in flux component q_z along a specified line on the small pipe surface.

$$T = x^3 + y^3 + z^3 - 3yx^2 - 3xz^2 - 3zy^2 \tag{17}$$

The inner evaluation points are uniformly distributed on the two line segments. The one line segment has endpoints at $(0.05,5,2)$ to $(4.95,5,2)$, and the other from $(5.05,5,2)$ to $(9.95,5,2)$. The boundary evaluation points are uniformly distributed on the isoparametric line segment with from $(\pi,0.05)$ to $(\pi,0.99)$ in the parametric space of the pipe surface. In this space, $\widehat{x} \in (0,2\pi)$ and $\widehat{y} \in (0,1)$. The numerical results together with reference solutions of the fluxes at internal points are shown in Fig. 8. It is seen the numerical results are in good agreement with the reference solutions, even at internal locations very close to the pipe surface (up to 0.02 away from pipe surface). Fig. 9 presents the variation of the flux component q_z along the specified line on the pipe surface. It is seen that the numerical results are also accurate, even though there is a slight deviation from exact solution at two ends and middle of the line. The reason for this deviation is that the approximation functions between neighboring tube elements are discontinuous. And there are only two tube elements used to approximate the field variables.

It should be pointed out that the hole radius is very small in this test. There is a ratio up to 800 of the maximum side length of the block to the minimal radius. The accurate numerical results have shown that the present method can deal with the holes with very small radii effectively.

Table 2
Mesh information, CPU time and memory requirements for the second example.

d/a	Method	Element number	Node number	CPU time (s)	Memory (MB)
0.2	BFM	387	1167	3	32.69
	BEM	456	2736	16	179.68
0.3	BFM	341	1029	3	25.42
	BEM	380	2280	11	127.78
0.4	BFM	281	849	3	17.31
	BEM	654	3924	23	369.58
0.5	BFM	245	741	2	13.12
	BEM	654	3924	23	369.58

4.2. Block with a larger cylindrical hole

For the purpose of studying the capacity of a singular tube element in capturing heat transfer pattern, the same $10 \times 10 \times 4$ block but with a larger cylindrical hole is used in this example. In this study, five cases with different values of d/a are considered (see Table 2), where d is the diameter of the hole, and a is the maximum side length of the block ($a = 10$). For each case, the boundary conditions are given as the same in the first test case of Section 4.1. The evaluation points are inside the block, which are uniformly distributed on the line segments with two endpoints at $(0.01,5,2)$ and $(4.99 - d/2,5,2)$. The distance from the second endpoint to the hole surface is only 0.01. This is to say that the point is very close to the hole surface.

Table 2 presents the mesh information and computational requirements for all cases used in the BFM and BEM. In the BFM models, the hole surface is modelled by a singular tube element with 9 nodes or 12 nodes, while all other surfaces are modelled by 3-noded linear triangular elements. In the BEM models, all surfaces are divided into 6-noded quadratic triangular elements. Fig. 10 shows the boundary elements employed in the case of $d/a = 0.2$. The new triangular elements with negative parts are not applied over the surfaces intersected by the hole, since the hole diameter is too large to be represented by the new elements.

Fig. 11 shows the results of fluxes at evaluation points obtained by the current method compared with the BEM results. It is clearly found that the there is a good agreement between the results, even at point very close to the hole surface. The discrepancy at the larger hole ratio is to expected, because the flux field around the hole is too complex to be represented by the very coarse surface mesh. Again, the heat concentration is well captured by a singular tube

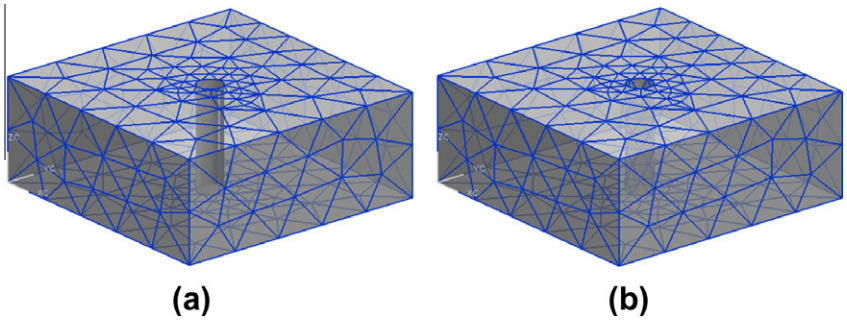

Fig. 10. Two types of boundary meshes for the block with a cylindrical hole of diameter $d = 2$. (a) BFM mesh with 387 elements and 1167 nodes. (b) BEM mesh with 456 elements and 2736 nodes.

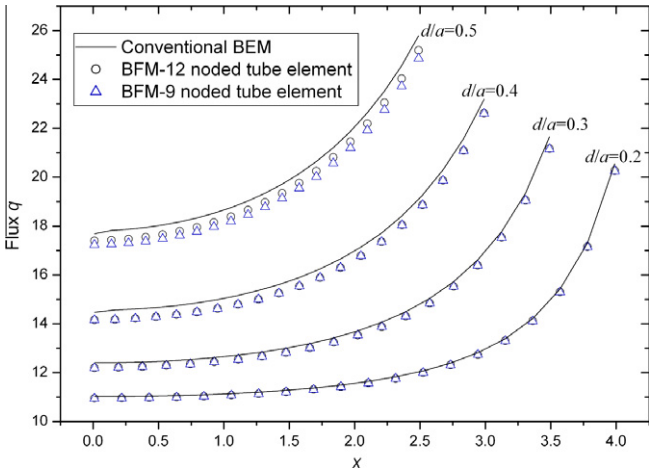

Fig. 11. Variation in flux q along the line segments for different values of d/a.

element in the cases of $d/a = 0.2, 0.3, 0.4$. The accepted results are also obtained in the case of $d/a = 0.5$. From Fig. 11, it is also observed that the results using a 12-noded tube element are better than that with a singular 9-noded element in the cases of the largest hole ratio. From the last two columns in Table 2, it is clear that computational costs used in the BFM are less than that of the conventional BEM.

4.3. Block with free shaped holes

Finally, we study the steady-state heat conduction in a $10 \times 10 \times 10$ block including a large number of small holes in the shape of free shaped tubes. This complicated structure is shown in Fig. 12(a). Fig. 12(b) depicts a local enlarged geometry. It is seen that these tubular holes are designed in different positions, although stretch in nearly the same direction. The total number of holes is 100. The radii of all the holes are identical and equal to 0.05. A Dirichlet problem is solved for which the essential boundary conditions are imposed on all the faces corresponding to Eq. (17). The all surfaces of this complicated structure are discretized with only 1994 boundary elements (totally 7782 nodes). Three slender tube elements are used for each tube. The required CPU time and memory for this problem are 1453.49 MB and 337 s, respectively.

Sample points are uniformly spaced on the isoparametric line segment from $(0.5, 0.05)$ to $(0.5, 0.95)$ of a pipe surface, for which two coordinate parameters $\hat{x}$ and $\hat{x}$ are set in the interval $[0, 1]$. Fig. 13 shows the numerical results of normal flux q and flux com-

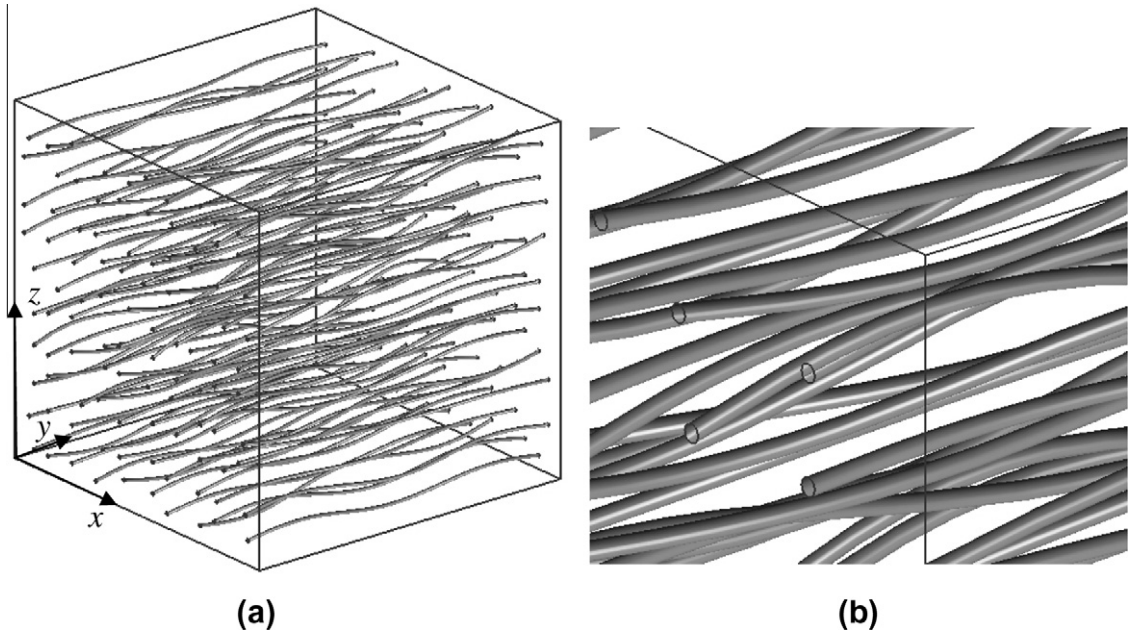

Fig. 12. A block with a large number of tubular holes. (a) The distribution of holes in the block. (b) A local enlarged geometry.

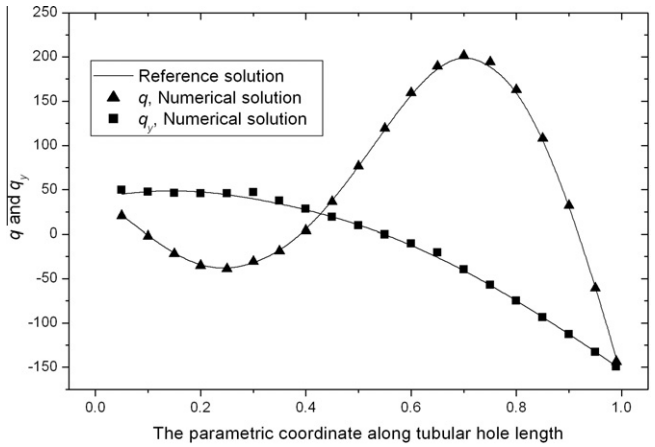

Fig. 13. Normal flux q and flux component q_y along the specified isoparamtric line on a tubular hole.

ponent q_y at the sample points. It is observed that numerical results are in excellent agreement with the reference solution. When the points are very close to the tube end, the results are also very precise. This indicated that it is reasonable and effective to utilize the elements with negative parts around the tube ends.

We should point out here that it is impossible to obtain a reasonable discretization with domain elements used in the FEM for this geometry. Much effort is also required to discretize all surfaces with high quality boundary elements in the BEM. However, in our method, two types of new discontinuous elements are used to describe tubular holes and their ends, which can be done very easily. It should be also pointed out each tubular hole is modelled by a NURBS surface in the CAD model of this complicated structure. The geometry information of the tubes, such as coordinates, can be directly available from the CAD model by making use of the Open API (Application Program Interface) of the CAD software.

5. Conclusions

Using the BFM, an effective numerical model for steady-state heat conduction analysis of solids with small open-ended tubular holes has been proposed. In order to describe these holes relative easily but keep exact geometry, two types of special surface elements have been developed, namely, the tube element and triangular element with negative parts. A free shaped hole can be represented by a small number of these elements instead of many fine boundary elements or approximation model with "hole element" in existing BEM models.

The analysis was shown to be very efficient as well as highly accurate for a range of problems. It was also shown that the local thermal concentration can be well captured by tube elements. An attractive feature of the present implementation lies in the fact that the tubular holes can be exactly modelled by a few of the proposed elements. Also, the radii of the holes can be changed without rebuilding the main BFM mesh, making reanalysis being taken easy. All features not only substantially simplify the discretization task for the solid with tubular holes, but also result in significant saving in computing cost and time. Thus, the present method is especially applicable for analysis of the solids with tubular holes or tubular fibers. Extending the method to be applied in study on the thermal behavior of the composites containing a large number of fibers is a subject for future research.

Acknowledgements

This work was supported in part by National Science Foundation of China under grant numbers 10972074 and 11172098, and in part by National 973 Project of China under grant number 2010CB328005.

References

[1] M.R. Barone, D.A. Caulk, Special boundary integral equations for approximate solution of potential problems in three-dimensional regions with slender cavities of circular cross section, IMA J. Appl. Math. 35 (1985) 311–325.
[2] G.F. Dargush, P.K. Banerjee, Advanced development of the boundary element method for steady-state heat conduction, Int. J. Numer. Methods Eng. 28 (1989) 2123–2143.
[3] D.P. Henry, P.K. Banerjee, Elastic analysis of three-dimensional solids with small holes by BEM, Int. Numer. Methods Eng. 31 (1991) 369–384.
[4] P.K. Banerjee, D.P. Henry, Elastic analysis of three-dimensional solids with fiber inclusions by BEM, Int. . Solids Struct. 29 (1992) 2423–2440.
[5] J. Chatterjee, D.P. Henry, F. Ma, P.K. Banerjee, An efficient BEM formulation for three-dimensional steady-state heat conduction analysis of composites, Int. J. Heat Mass Transfer 51 (2008) 1439–1452.
[6] F. Ma, J. Chatterjee, D.P. Henry, P.K. Banerjee, Transient heat conduction analysis of 3D solids with fiber inclusions using the boundary element method, Int. J. Numerical Methods Eng. 73 (2008) 1113–1136.
[7] C.B. Federico, J.M. Rogerio, A family of hole boundary elements for modeling materials with cylindrical voids, Eng. Anal. Boundary Elem. 32 (2008) 578–590.
[8] J.M. Zhang, X.Y. Qin, X. Han, G.Y. Li, A boundary face method for potential problems in three dimensions, Int. J. Numer. Methods Eng. 80 (3) (2009) 320–337.
[9] X.Y. Qin, J.M. Zhang, G.Y. Li, X.M. Sheng, Q. Song, D.H. Mu, An element implementation of the boundary face method for 3D potential problems, Eng. Anal. Boundary Elem. 34 (2010) 934–943.
[10] Y.X. Mukherjee, S. Mukherjee, The boundary node method for potential problems, Int. J. Numer. Methods Eng. 40 (1997) 797–815.
[11] M.K. Chati, S. Mukherjee, The boundary node method for three-dimensional problems in potential theory, Int. J. Numer. Methods Eng. 47 (2000) 1523–1547.
[12] J.M. Zhang, Z.H. Yao, H. Li, A hybrid boundary node method, Int. J. Numer. Methods Eng. 53 (2002) 751–763.
[13] J.M. Zhang, Z.H. Yao, Meshless regular hybrid boundary node method, Comput. Model. Eng. Sci. 2 (2001) 307–318.
[14] Y.J. Liu, Analysis of shell-like structures by the boundary element method based on 3-D elasticity: formulation and verification, Int. J. Numer. Methods Eng. 41 (1998) 541–558.